phys. stat. sol. (b) **217**, 545 (2000)

Subject classification: 61.72.Lk; 62.20.−x; 71.15.−m; S5.11

Modeling Brittle and Ductile Behavior of Solids from First-Principles Calculations

U. V. WAGHMARE (a), E. KAXIRAS (a), and M. S. DUESBERY[1]) (b)

(a) Department of Physics, Harvard University, Cambridge, MA 02138, USA

(b) Fairfax Materials Research, Fairfax, VA 22153, USA

(Received August 10, 1999)

A broad classification of solids in terms of their mechanical behavior would characterize them as brittle or ductile. While there is no doubt that ultimately this behavior is due to processes at the atomistic level, the link between these processes and their macroscopic manifestation is difficult to establish. Phenomenological theories that try to address this link must rely on microscopic parameters, the values of which are beyond their scope. Here we review recent efforts to employ first-principles electronic structure calculations in order to determine important physical quantities which, in conjunction with phenomenological theories, can provide insight into brittle versus ductile behavior. We apply this approach to cases of intrinsic interest, such as silicon, the prototypical brittle solid, as well as in cases of practical interest, such as the improvement of ductility in molybdenum disilicide, a material of potential usefulness in improved turbine blades. Current indications are that this combination of techniques can serve as powerful qualitative predictive tool for the dependence of mechanical behavior on the microscopic structure and chemical composition of a solid.

1. Introduction

Mechanical properties are at the core of many uses of materials in traditional as well as high technology applications. Solids are typically classified as brittle or ductile, according to how they respond to external loads. For example, brittle failure is a singular limiting factor in the application of advanced materials in components ranging from electronic devices to turbine engine blades. In brittle solids, the imposition of external stress results in the extension of pre-existing cracks: the stress concentration at the crack tip (which actually diverges for a sharp tip, when calculated within continuum elasticity theory [1]), leads to bond-breaking and cleavage. In contrast to this, in a ductile substance the large stress at the crack tip is absorbed by generation and motion of dislocations which blunts the crack; the net effect is plastic deformation of the material but no breaking. In advanced electrical and mechanical devices, as the size of critical components shrinks, and the demands for high performance and reliability increase, a detailed understanding of the microscopic processes responsible for ductile or brittle behavior becomes increasingly important. Understanding such processes at the atom-

[1]) We are saddened to report that Dr. M. S. Duesbery passed away during the preparation of this manuscript. Dr. Duesbery's contributions to the understanding of mechanical properties of solids have left an indelible mark on the field. The two other authors feel indebted to Dr. Duesbery for generously sharing with them his deep knowledge of this field and for his invaluable contributions to this collaboration.

istic level and connecting them to the macroscopic behavior of real materials will provide unprecedented level of control in the design of new applications.

What would it take to actually simulate at the microscopic level the processes responsible for brittle or ductile behavior? We would need to include in the simulation a large enough number of atoms to capture the different types of defects (cracks, dislocations, surfaces, grain boundaries, point defects) and their response to external loading, at finite temperature. For a solid of linear size one micron this requires the simulation of the dynamic behavior of $\approx 10^{12}$ atoms in a variety of local environments and for times that are very long compared to the time scale of atomic vibrations (which sets the scale for each step in the simulation). This is impossible with current computational capabilities. But even if it were possible, the sheer volume of data generated by following the evolution of 3×10^{12} degrees of freedom for millions of simulation steps, would make it difficult to analyze and comprehend the results. At present, supercomputers can be employed to simulate the behavior of up to 10^9 atoms, using the simplest type of interatomic interaction (referred to as classical potentials). In this approximation, the complex interaction between atoms through the valence electrons responsible for the cohesion of solids, is reduced to a few-body (typically two- and three-body) interatomic potential which depends on atomic distances and the angles between such distances. It is not clear to what extent this simplified description can capture realistically the atomistic processes responsible for bond breaking and cleavage (in the case of a brittle solid) or dislocation nucleation and motion (in the case of a ductile solid). Even if this can be successfully done for a solid consisting of a single element (where a sophisticated interatomic potential might have a chance at performing reasonably), when many types of atoms are present and chemical interactions become dominant at the microscopic level, this approach would quickly run up against insurmountable difficulties.

Alternatively, one can use sophisticated quantum mechanical methods for describing the properties of solids at the atomic level. When these methods are entirely self-reliant, i.e. they do not depend on any parameters that cannot be determined within the theory (other than fundamental physical constants), they are referred to as first-principles approaches. For instance, quantum mechanical methods based on Density Functional Theory [2] have proven to be powerful and unbiased tools for microscopic studies of a wide range of materials properties. Direct application of these methods yields an accurate description of the electronic and atomic structure of bulk crystals, their simple surfaces and interfaces, of small clusters of atoms, etc. Properties that represent small perturbations from the equilibrium crystal structure of the solid, such as the phonon spectrum, elastic moduli, optical, dielectric and magnetic constants, can also be obtained with reasonable accuracy. This is possible because all these properties can be modeled by a small number of atoms, since these calculations are limited to systems of order a few hundred atoms. At present it is entirely out of the question (and, if feasible, might represent a waste of valuable computational resources) to try to simulate systems with millions or billions of atoms using first-principles quantum mechanical calculations.

It is clear from the above discussion that successful modeling of physical phenomena which involve atomistic processes and their implications for macroscopic behavior, must rely on a combination of methodologies. A very active field of "multiscale modeling" of materials behavior has emerged recently from this realization. Several ways to implement multiscale modeling, with different strengths and weaknesses, have been put for-

ward. It is beyond the scope of the present article to review these approaches. Here we aim to present one of the simplest ways of linking information between the microscopic and macroscopic realms, and explore its potential to address real problems in materials behavior. Although admittedly simple and limited, this approach offers some intriguing insight to complex phenomena such as brittle versus ductile failure, and can have predictive capabilities within a well defined scope of applications. The essence of this approach is to use results from phenomenological macroscopic theories (based on continuum elasticity) coupled with first-principles quantum mechanical calculations to determine the values of any physical parameters that enter in the phenomenological description.

The article is organized as follows: Section 2 covers the theoretical background behind the model we use to assess ductile and brittle response from a macroscopic phenomenological perspective. The first-principles quantum mechanical methods which we use to obtain the model parameters are reviewed in Section 3. In Section 4, we discuss applications of this approach to mechanical behavior of real materials: silicon, the prototypical brittle solid, and molybdenum disilicide and its substitutional alloys, which represent a class of materials with potentially important applications. We conclude in Section 5 with a discussion of the approximations inherent in our approach and the consequent limitations.

2. Brittle versus Ductile Behavior: Macroscopic Theory

In this section, as a preamble to subsequent discussion, we first introduce the concept of the generalized stacking fault energy surface (γ-surface) and indicate how it relates to dislocation nucleation and mobility. We also review theories of the Ductile–Brittle Transition (DBT), particularly emphasizing their connection with dislocation nucleation and mobility, and therefore the γ-surface.

2.1 The generalized stacking fault energy

The concept of the γ-surface, originally introduced by Vitek [3], is central to many macroscopic theories of plastic deformation. Consider a crystal cut into two halves parallel to the (*hkl*) crystallographic plane and suppose that one half is displaced relative to the other by a vector $\mathbf{v}$. The plane (*hkl*) is called the fault plane and $\mathbf{v} = 0$ corresponds to the ideal crystal, the minimum energy configuration. The change in energy per unit area of the crystal as a function of $\mathbf{v}$, which is varied on the (*hkl*) plane to scan a unit cell, is called the γ-surface. If the atoms in the crystal are allowed to relax for an arbitrary $\mathbf{v}$, the fault (or γ-surface) is called relaxed. The γ-surface contains a wealth of information about the crystal: at the atomistic level, it can be used to predict dislocation core properties [4]; at the macroscopic level it can yield the stress intensity at which dislocations are nucleated at the crack tip [5]. The γ-surface is a fundamental material property which can be obtained from atomistic calculations.

2.2 Dislocation motion

When dealing with dislocations from the macroscopic perspective, some phenomenological description consistent with the continuum picture of a solid must be invoked. A useful description of this type was put forward by Peierls [6] and Nabarro [7]. The

Peierls-Nabarro model represents the crystal dislocation as a continuous, planar distribution of infinitesimal disregistry of atomic planes on either side of a fault plane. The density of this disregistry, $\varrho(x)$ is given in terms of the displacement field $\mathbf{u}(x)$ as $\varrho(x) = |\mathrm{d}\mathbf{u}/\mathrm{d}x|$. The balance between the forces among the infinitesimal segments of the dislocations and the elastic restoring force of the crystal leads to the Peierls-Nabarro integro-differential equation

$$K \int_{-\infty}^{\infty} \mathrm{d}x' \frac{\mathrm{d}\mathbf{u}(x')}{\mathrm{d}x'} \frac{1}{(x - x')} = -\nabla_{\mathbf{u}}(\gamma(\mathbf{u}(x))) \,, \tag{1}$$

subject to the normalization condition

$$\int_{-\infty}^{\infty} \frac{\mathrm{d}\mathbf{u}(x)}{\mathrm{d}x} \mathrm{d}x = \mathbf{b} \,. \tag{2}$$

Here, K is an elastic constant (its exact value depends on the nature of the dislocation) and $\mathbf{b}$ is the Burgers vector of the dislocation (it is assumed for simplicity that we are dealing with a straight infinite dislocation and the disregistry is only along one direction x, perpendicular to the dislocation line). Eq. (1) relates the stress on the lattice at a position x due to the infinitesimal dislocation distribution at that point $\mathbf{u}(x)$ to the force exerted by the lattice due to its distortion, given by the gradient of the γ-surface. Eq. (2) normalizes the total misfit to the Burgers vector (for more details see, for example, Hirth and Lothe [8]).

In order to determine the effects of dislocation motion, we need to consider what will happen within this picture when this distribution of lattice disregistry is moved by a distance equivalent to the lattice periodicity and compute the change in energy as a function of x. This energy cost can then be related to the external stress required to move the dislocation. This energy is referred to as the Peierls energy $W_{\mathrm{P}}(x)$ and its maximum gradient is the Peierls stress for translation of rigid dislocations at zero temperature. While extremely useful as a conceptual tool, this model has many limitations. The method has been shown to predict Peierls stresses much larger than those determined from a fully atomistic calculation [9, 10]. One of the important limitations, for example, is the neglect of any change in $\varrho(x)$ with position during motion through lattice; if this constraint is removed, the agreement with atomistic methods is improved substantially [11]. For a rough estimation of the Peierls stress, the step in which the distribution is translated through the lattice can be bypassed: it has been shown that, in the limit of narrow dislocations, the Peierls stress is given directly by the maximum gradient of the γ-surface along an extremal path (the lowest energy path between endpoints corresponding to ideal crystal) over which the displacement vector $\mathbf{v}$ varies continuously from 0 to $\mathbf{b}$ [12].

2.3 Ductility versus brittleness

As mentioned in the introduction, the competing processes which lead to brittle or ductile behavior are the extension of the crack by creation of fresh surfaces (brittle response) or the generation of dislocations that exert a back stress which reduces, and thus *shields* the stresses by blunting the crack tip (ductile response). Most solids can

undergo a transition between brittle and ductile response, which can be very sharp as a function of temperature (in bulk silicon the transition takes place for a change in temperature of a couple of K!). In brittle failure, the energy required for an incremental advance of the crack front is

$$G = 2\gamma_s \,, \tag{3}$$

where G is the energy release rate (the mechanical energy released per unit area swept by the crack front) and γ_s is the surface energy (the energy needed to create a unit area of fresh surface). This is known as the Griffith criterion [13]. For ductile response a more complex picture needs to be invoked, taking into account dislocation nucleation and motion, in the neighborhood of the crack tip.

The first attempt to rationalize the distinction between brittle and ductile behavior was made by Kelly and coworkers [14], who postulated that a material would be ductile if the crack tip stress exceeded the theoretical shear stress before the theoretical tensile stress was reached. This work did not address the DBT. A direct linkage to the DBT was made later by Rice and Thomson [15], who proposed that the onset of ductile behavior occurred when spontaneous emission of dislocations at the crack tip became feasible. In the RT model, dislocations which move more than a critical distance a_c from the crack tip are repelled by the crack and are hence considered to be nucleated. If a_c is smaller than the dislocation core radius a_0, the material is considered to be ductile at all temperatures; on the other hand, if $a_c > a_0$, the material is brittle at low temperatures. The linkage of the RT model with dislocation energy naturally introduces a temperature-dependene DBT. Unfortunately, it predicts rather large activation energies for dislocation nucleation in brittle materials, precluding a DBT significantly below the melting temperature T_m. Experimentally, the DBT is found to occur at much lower temperatures, for example, at $(2/3)T_m$ for Si.

There are three more recent theories to describe the DBT. In a modern variant of the RT model, Rice [16] introduced the unstable stacking fault energy γ_{us} as the maximum energy barrier encountered along the extremal path (introduced in the previous subsection) connecting 0 and **b** on a plane (*hkl*). Rice showed that γ_{us} is a measure of the nucleation energy for a dislocation of Burgers vector **b** on the (*hkl*) plane. Within the Rice model, the criterion for dislocation nucleation at the crack tip, and therefore ductility, is reached when

$$G = \alpha\gamma_{us} \,, \tag{4}$$

where α is a constant which depends on the geometry of the crack, but is of the order unity. We point out a connection between γ_{us} and the Peierls stress (the former being the maximum energy and the latter being the maximum slope along the extremal path). If the energy has a sinusoidal form, the maximum slope will scale with the maximum energy, implying that the Peierls stress should scale directly with γ_{us}.

In an alternative model of the DBT, Hirsch and Roberts (HR) [17] postulate that the governing mechanism is the motion, rather than the nucleation of dislocations. The crack tip stresses are presumed to activate internal sources, with dislocations of one sign moving into the bulk and of the opposite sign being absorbed into the crack. Of course, absorption of dislocations of one sign is equivalent to emission of dislocations with opposite sign. The HR theory therefore connects the DBT with dislocation mobility. This, as shown above scales with the unstable stacking fault energy γ_{us}.

Yet a different model, due to Khantha, Pope, and Vitek (KPV) [18], argues that the shielding dislocations are nucleated in the vicinity of the crack tip as a self-screening cloud of dipoles by a Kosterlitz-Thouless type mechanism [19]. In this case, the key quantity is the total dislocation energy, as in the RT model. However, the elastic energy contribution is much smaller due to the smaller screening length of the KPV model, while the contribution of the dislocation core energy is the same as in the RT model. It is precisely the dislocation core region in which the misfit assumes the magnitude at which the γ-surface reaches the unstable stacking fault value; i.e. the core energy depends on the unstable stacking fault energy. Thus, although the specific details of the KPV model are quite different from either the Rice or the HR model, γ_{us} can be considered to be the key parameter for dislocation related processes of ductility in all three models.

To summarize, the conditions for both brittle fracture and the nucleation and motion of dislocations can be expressed in terms of features of the γ-surface. If we adopt the view that dislocation nucleation is a necessary precursor to dislocation motion, the conditions become particularly simple, depending only on the two energies γ_s and γ_{us}. It is tempting to try to use these simple arguments to characterize the tendency of a solid to behave as a brittle or a ductile substance. Brittle behavior is the consequence of the condition of eq. (3) being satisfied before the condition of eq. (4); if the converse is true, the material will be ductile. More specifically, we can define a "disembrittlement parameter"

$$D = \frac{\gamma_s}{\gamma_{us}} , \tag{5}$$

the value of which will determine to which class a solid belongs. The difficulty with using this criterion is that values for γ_s and γ_{us} are not provided by any analysis based on continuum arguments of the type invoked in this section. They have to be established from accurate microscopic calculations. Even then, it is not clear for which slip system (i.e. the combination of fault plane and Burgers vector of dislocation) or for which cleavage plane, these quantities must be evaluated. Moreover, the value of D that corresponds to the DBT is not known with any precision. This critical value has been estimated [16] to be between 1 and 10. One might hope, however, that *changes* in the value of D due to changes in the microscopic structure or chemical composition of a solid will correlate with changes in the solid's tendency to behave as a brittle or a ductile substance. It is this idea that we pursue below.

3. First-Principles Methods

The minimal empirical input for the study of equilibrium properties of a solid is its composition and its atomic structure. At $T = 0$, the optimal structure can be determined by calculating the total energy and finding the minimum energy structure. First-principles methods can provide an accurate determination of the total energy as a function of structure and composition. They can therefore be employed to determine either the optimal structure given the composition and certain external conditions (like pressure), or to determine the energy difference between specific structures of interest. Below we will use such methods to obtain accurate values for γ_s and γ_{us}.

First-principles methods are typically based on the adiabatic approximation (or Born-Oppenheimer approximation), by treating electrons in their quantum mechanical

ground state for a given configuration of nuclei $\{\mathbf{R}_i\}$. As a result, the energy of a given state is given by the sum of the electronic ground state energy $E_{0-\mathrm{el}}(\{\mathbf{R}_i\})$ and the ion–ion interaction (Coulomb) energy E_{ion} obtained by an Ewald summation:

$$E_{\mathrm{tot}} = E_{0-\mathrm{el}}(\{\mathbf{R}_i\}) + E_{\mathrm{ion}} \,. \tag{6}$$

Detailed descriptions of many of the commonly used first-principles methods are presented in other parts of the present collection of review articles (see [20]). Here, we briefly highlight some of the essential features of the methods based on Density Functional Theory, and discuss their use in studying mechanical behavior through total energy calculations. More than 99% of the computational effort is spent in the calculation of the electronic ground state.

The problem of finding the quantum mechanical ground state of electrons in solids is a many-body problem. While highly accurate methods exist for solving this many-body problem, such as quantum Monte Carlo, these can handle only very small systems of order tens of atoms at most. For larger systems of interest, approximate but reasonably accurate schemes that make calculations feasible with existing computational facilities are mostly based on density functional theory (DFT) [2]. The central theorem of DFT, proven by Hohenberg and Kohn, states that the ground state energy of an electronic system is a unique functional of its charge density $\varrho(\mathbf{r})$ and is variational (minimum) with respect to the charge density: for the ground state of a system of electrons in an external potential $V_{\mathrm{ext}}(\mathbf{r})$,

$$E[\varrho(\mathbf{r})] = \int \mathrm{d}\mathbf{r} V_{\mathrm{ext}}(\mathbf{r})\varrho(\mathbf{r}) + \frac{1}{2}\int\int \mathrm{d}\mathbf{r}\mathrm{d}\mathbf{r}' \frac{\varrho(\mathbf{r})\varrho(\mathbf{r}')}{|\mathbf{r}-\mathbf{r}'|} + F[\varrho(\mathbf{r})] \tag{7}$$

is a minimum with respect to variations in $\varrho(\mathbf{r})$, under the constraint that

$$\int d\mathbf{r}\varrho(\mathbf{r}) = N \,, \tag{8}$$

where N is the total number of electrons. The functional $F[\varrho(\mathbf{r})]$ contains the kinetic and exchange-correlation energies for interacting electrons. This functional is not known exactly and its use in practice generally involves an approximation called the local density approximation (LDA): the ground state energy is a local functional of the total charge density. This functional is derived using results of more elaborate approaches (such as the Random Phase Approximation or Quantum Monte-Carlo simulations) for the homogeneous electron gas [21]. Kohn and Sham [2] expressed the charge density in terms of single particle wavefunctions and mapped the ground state problem in DFT onto a single particle problem in an effective potential that must be determined self-consistently.

The basis set used to represent the Kohn-Sham wavefunctions and the electronic charge density in this work consists of plane waves with kinetic energy smaller than a fixed energy cutoff determined by the problem of interest. We make use of the translational symmetry of bulk crystals through Bloch's theorem, so that the wave vector $\mathbf{k}$ in the Brillouin zone (BZ) labels an electronic eigenfunction, and the cell periodic part of the wavefunction can be expressed in terms of a discrete set of plane waves generated as multiples of the reciprocal space vectors. The plane wave basis set allows for efficient calculation of the various operator matrix elements, including the energy and the forces on the ions (obtained through the Hellmann-Feynman theorem) and an unbiased representation of charge densities.

Another simplifying approximation is the use of pseudopotentials [22] to represent the ion–electron interaction. Thus the core electrons in an atom are frozen and are replaced by an effective potential which is what the valence electrons experience. With this, the full nuclear Coulomb potential Z/r, with Z the atomic number and r the radial distance from the nucleus, is replaced by a pseudopotential which behaves as Z_v/r outside a cutoff radius r_c but remains finite as $r \to 0$, with Z_v the valence charge. The pseudopotential is constrained to ensure that: 1. the lowest s, p, and d orbital energy eigenvalues of the pseudoatom are identical to the valence electron eigenvalues of the full atom, 2. the normalized radial eigenfunctions of these levels are identical beyond r_c to those of the valence electrons in the full atom, 3. the logarithmic derivatives of the pseudo-wavefunctions, evaluated at r_c and the valence electron eigenvalue, are the same as those of the valence wavefunctions of the real atom. These constraints are designed to make the lowest energy states of the pseudoatom identical to those of the valence states of the real atom outside the cutoff radius, which is the region where valence wavefunctions overlap to produce bonding between the atoms in a solid.

The first advantage of using a pseudopotential is the elimination of core electrons, which hardly affect the bonding in solids. A second advantage is that the eigenfunctions of the valence electrons are replaced by nodeless pseudo-wavefunctions, whose representation in a plane wave basis is easier. In certain cases, like first row elements and transition metals, for which the valence p and d wavefunctions are already nodeless and localized, additional consideration is required. The constraints on a pseudopotential mentioned above are not sufficient to completely determine its form for $r < r_c$. This freedom can be used to optimize a pseudopotential, so that the corresponding pseudo-wavefunctions can be represented with a basis set truncated with a relatively low energy cutoff [23]. This class of pseudopotentials, called "optimized pseudopotentials", is used for first-row elements and transition metals in the present work. As a test of these pseudopotentials, our calculations of ideal crystal properties for these elements give lattice constants within 2% of their experimental values.

For the plane wave basis, an energy cutoff up to 60 Ry for solids containing transition metals and oxygen and 12 Ry for Si has been used in the present calculations; these computational parameters ensure convergence of energy differences between different structures to within 1 mRy/atom. A Fermi-Dirac broadening scheme with $k_B T = 0.04$ eV is used to represent the Fermi surface discontinuity. We sample the Brillouin zone using the Monkhorst-Pack scheme [24] with k-point grids of $6 \times 6 \times 6$ for bulk Si (an f.c.c. lattice with a 2-atom basis) and $7 \times 7 \times 7$ for bulk $MoSi_2$ (a b.c.t. lattice with a 3-atom basis), the other brittle solid studied. For the calculation of the γ_s and γ_{us} we use slab configurations (see Fig. 1), with multiples of the unit cell along the slab direction and proportionately smaller grids of k-points in the corresponding direction in reciprocal space. For efficient calculations on metallic systems involving large unit cells and surfaces, we use a preconditioned conjugate gradient algorithm [25] to iteratively diagonalize the Kohn-Sham Hamiltonian and the Kerker charge density mixing scheme [26] in the self-consistent procedure to avoid sloshing of charge between the vacuum and the slab region. This scheme mixes small wave vector components of the charge density gradually and thereby damps oscillations during the self-consistency cycle.

Surface energies γ_s are obtained from the difference between the total energy E_{tot} of a crystal cleaved across a given plane and of the bulk (see Fig. 1). We consider a periodic supercell containing several units of the ideal crystal cell (6 for Si, 2 to 4 for

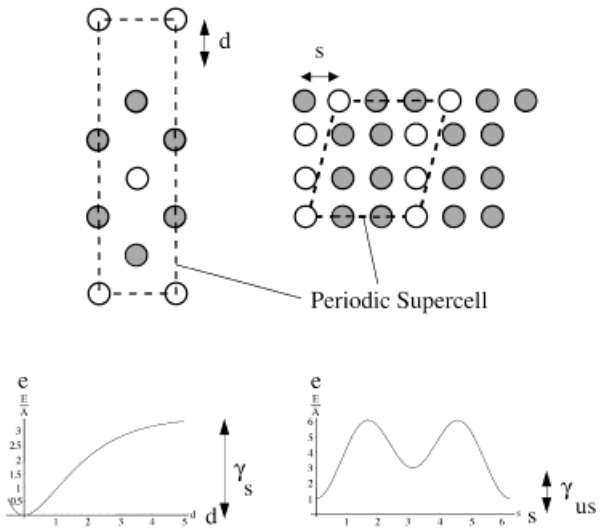

Fig. 1. Geometry of supercells in a typical calculation of surface energy γ_s and unstable stacking fault energy γ_{us}

$MoSi_2$) and calculate the total energy as a function of d, the distance between two atomic layers separated by the desired cleavage plane in the supercell. These energies are fit to the universal binding energy function [27]

$$e(d) = \frac{E_{\text{tot}}(d)}{A} = e_\infty - 2\gamma_s(1+f)\mathrm{e}^{-f} \,, \tag{9}$$

where $f = (d - d_0)/\lambda$, e_∞ is the energy per unit area (A) of the cleaved crystal, d_0 is the inter-planar separation in the ideal bulk crystal and λ a fitting parameter. The unstable stacking fault energy is obtained from the total energy of a supercell containing the fault plane with the two halves of the cell displaced in the direction of the fault vector with respect to each other (see Fig. 1).

4. Applications: Ductile versus Brittle Behavior

4.1 Silicon

In addition to its extensive use in technological applications (especially in the area of electronic devices), silicon also serves as the theorist's prototypical, covalently bonded, brittle solid. Si undergoes a brittle to ductile transition with increasing temperature, at 873 K. A remarkable feature of this transition is its sharpness (it has a width of approximately 2 K). It would be desirable to understand this transition at a microscopic level. This, however, may be beyond current capabilities of simulating all the necessary features, which include the nucleation and motion of dislocations near crack tips in various geometries, such as the formation of dislocation loops near the kinks of cracks, etc. Instead, we will discuss here recent efforts to establish some of the important characteristics of Si as obtained from first-principles atomistic scale calculations, like the values of γ_{us} on different fault planes. As discussed above, these quantities are relevant to macroscopic phenomenological theories of brittle versus ductile behavior.

In Si, the relevant fault plane is the {111} slip and cleavage plane. The crystal structure of Si, the diamond cubic lattice, allows for two distinct placements of the slip

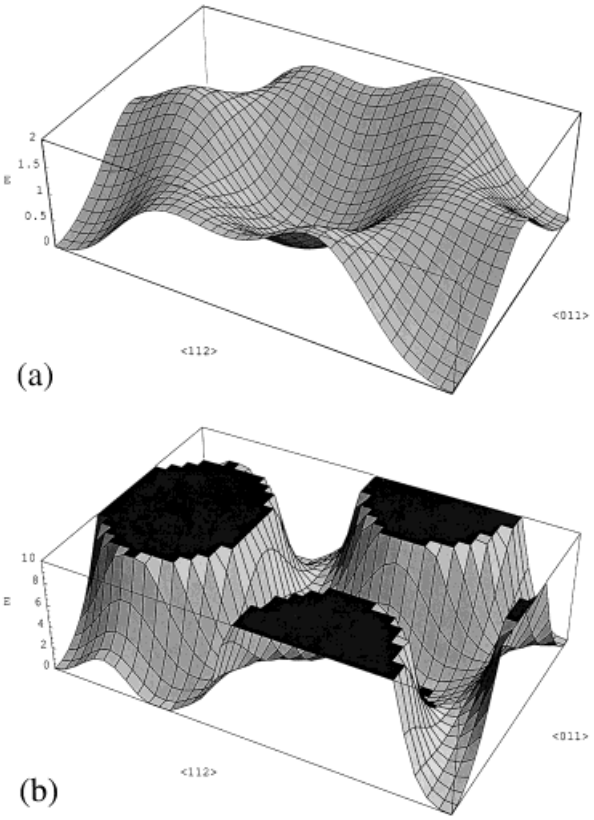

Fig. 2. Generalized stacking fault energy surface for a) the shuffle and b) the glide plane of Si

plane: a) between atomic planes that are separated by a distance equal to the nearest neighbor distance (that is, bisecting the Si–Si bond along the [111] crystallographic direction), b) between atomic planes that are separated by one third of the nearest neighbor distance. The two slip planes between a) widely spaced and b) narrowly spaced atomic layers are referred to as "shuffle" and "glide" planes in the context of dislocation motion [8].

Kaxiras and Duesbery [28] obtained the generalized stacking fault energy surface for both shuffle and glide planes using first-principles calculations in the DFT/LDA framework. The generalized stacking fault energy surfaces for these two planes are reproduced in Fig. 2a and b. We summarize their results for the unstable stacking fault energies in Table 1. While the values of γ_{us} are comparable in magnitude for the two slip

Table 1
Energy of unstable stacking faults, γ_{us} (in J/m^2), at various levels of relaxation, for the shuffle and glide planes in Si

	no relaxation	atomic relaxation at ideal volume	atomic relaxation and volume relaxation
a) shuffle	1.84	1.81	1.67
b) glide	2.51	2.02	1.91

planes, the energy scales are vastly different. It is clear from Table 1 that atomic relaxation affects the glide plane energetics more than the shuffle plane. This is not surprising because sliding on the glide and shuffle planes involves breaking of three and one bonds, respectively, per pair of atoms on either side of the slide plane. This indicates that at zero temperature the sessile mode will be favored. The same work attempted to generalize the concepts outlined in Section 2 to finite temperature based on the Vineyard [29] transition state theory for diffusion. With access to the entire generalized stacking fault (GSF) energy surface for slip, the problem can be mapped to that of a classical particle moving on a two-dimensional potential energy surface. This mapping involves folding all the degrees of freedom of the many-atom system to two collective degrees of freedom describing motion on the slip plane. The formulas for calculating entropy associated with the diffusion of a particle in transition state theory can then be used to obtain the entropy associated with the slip process, and from that the associated free energy at finite temperature. It was found that although the glide plane has a higher γ_{us} value, it also has higher entropy. Since the entropy term enters into the free energy with a negative sign, it is possible that under the proper thermodynamic conditions the free energy of the glide plane can become *lower* than that of the shuffle plane. Thus, as the temperature is increased beyond a critical point, a transition from sessile shuffle mode to glissile glide mode can occur. Kaxiras and Duesbery suggested that this change of preferred sliding mode could be related to the ductile to brittle transition in Si. The entire GSF energy surface can also provide useful information about the shape and Peierls stress associated with various dislocations [12, 30]. Juan and Kaxiras [30] calculated various GSF energy surfaces for silicon from first principles and obtained its dislocation properties.

While Rice's criterion for ductile versus brittle behavior addresses the issue of dislocation nucleation and motion, it does not include any information about the surfaces created due to dislocation emission at the crack tip. Juan, Sun, and Kaxiras (JSK) [31] introduced a correction to account for the surface traction effects, which they called the ledge surface contribution. Since the surface exposed near the tip of the crack upon nucleation of a dislocation is not equivalent to a free surface, including these effects in a criterion for brittle versus ductile behavior is quite demanding and can be done accurately only with first-principles calculations. For the case of Si, JSK were able to identify a geometry that allowed the calculation of the ledge surface contribution: they found that the energy associated with ledge surface creation is approximately 60% of the energy of the free surface. Assuming an evanescent force law, they incorporated the ledge effects into Rice's original theory within continuum mechanics, which showed that in silicon the increase in the necessary loading for dislocation emission due to surface traction can be up to 20%.

4.2 Molybdenum disilicide and its substitutional alloys

Experimental background: Molybdenum disilicide, $MoSi_2$, is a metalloceramic material with the strength of a ceramic and the toughness of a metal. It has a high melting point that makes it a promising candidate for high temperature turbine applications. The negative side to its use is that it becomes brittle below 1000 °C and loses its toughness. There are ongoing experimental efforts to disembrittle $MoSi_2$ at low temperatures. Several attempts to improve the low-temperature fracture toughness of $MoSi_2$ by forming

composite materials have been made. The addition of ceramic particles or whiskers such as SiC [32] or ZrO_2 [33] inhibits fracture and increases the fracture toughness to a level achieved by incorporation of a ductile second phase. For example, Mo in $MoSi_2$ [34] increases the fracture toughness (up to $\approx$10 MPa $m^{1/2}$). This is believed to be due to the crack-slowing effects of large matrix-particle interfacial stresses. The addition of carbon [35] scavenges silica from the grain boundaries, changing the fracture mode from intergranular to transgranular and increasing fracture toughness to 12 MPa $m^{1/2}$. The addition of carbon-lubricated silicon carbide continuous fibers increases the fracture toughness [36] to 35 MPa $m^{1/2}$ for cracks normal to the fiber length. Unfortunately, the toughness for cracks running parallel to the fibers is unaffected. This process is costly and not easily extended to three dimensions, making it an unsuitable candidate for practical use. The effect of structural modification on the DBT in $MoSi_2$ has also been examined, but the conclusions are conflicting.

There has also been some experimental work, similarly inconclusive, on the effect of chemical alloying. There are many choices to be tried for alloying, both in terms of choice of chemical element and of the concentration. Theoretical analysis can complement experimental efforts and indicate which type of alloying may *intrinsically* improve the material. Even using theory to eliminate some of the possible options can be very helpful in making experimental efforts cost-effective. Here, we present our analysis of ductile versus brittle behavior of $MoSi_2$ based on first-principles calculations.

Crystal structure: $MoSi_2$ crystallizes in a body centered tetragonal structure as shown in Fig. 3a, formed by the alternate stacking of single Mo and double Si (001) layers. Both Mo and Si atoms are highly coordinated, with 10 nearest neighbors; as expected with this level of coordination, $MoSi_2$ has metallic character. It has been found experimentally that many slip systems in $MoSi_2$ remain active at low temperatures [37]. Brittle failure in single crystals occurs only when the stress axis is close to [001] and is

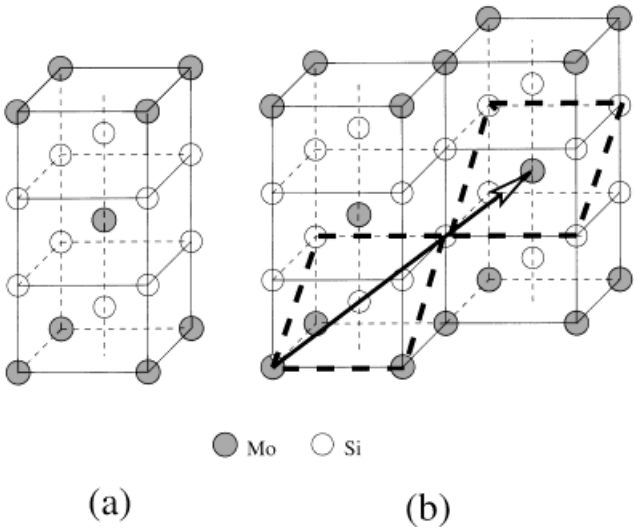

Fig. 3. Crystal structure of $MoSi_2$. a) Unit cell for the body centered $C11_b$ crystal; solid circles represent Mo atoms and open circles represent Si atoms. b) (013) plane and the Burgers vector for the slip system (013)[331]

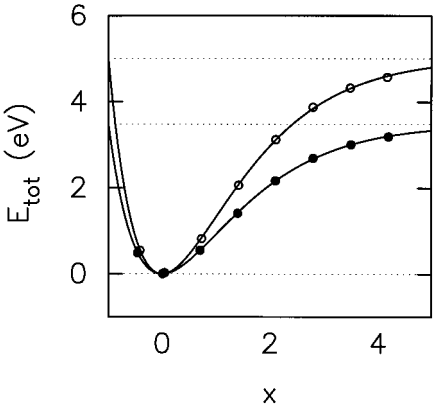

Fig. 4. First-principles energies (symbols) fitted to the universal equation of state (solid lines), for cleavage separating Mo–Si (open circles) and Si–Si (filled circles) planes of $MoSi_2$. x is the distance between the two adjacent atomic layers in the units of the length scale parameter λ (see text for details)

caused by increasing difficulty in the operation of the slip system $\{013\}\langle 331\rangle$, shown in Fig. 3b. This slip system involves motion of dislocations with $\frac{1}{2}[331]$ Burgers vector on (013) planes. To assess ductility trends, we calculate γ_s for (001) cleavage planes and γ_{us} for the $\{013\}\langle 331\rangle$ slip system from first principles.

Cleavage: In $MoSi_2$, there are two types of (001) cleavage planes: one separating adjacent layers of Si atoms and another separating adjacent layers of Mo and Si atoms. We use a supercell consisting of six atomic layers in the (001) direction (the conven-

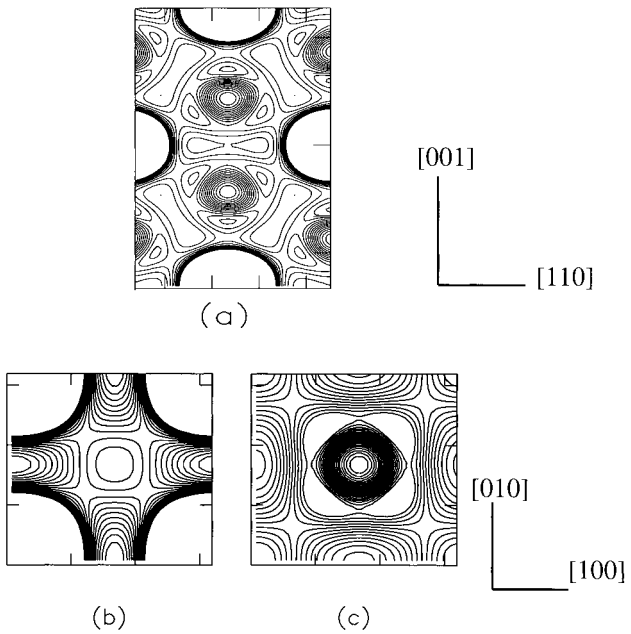

Fig. 5. Electronic charge densities of $MoSi_2$ in a) the (110) plane which contains both Si and Mo atoms, b) the (001) plane of Mo atoms, and c) the (001) plane of Si atoms. In a), Mo atoms are at the center of closely spaced large circular contours and Si atoms at the center of sparsely spaced elliptic contours. In b), Mo atoms are at the corner of the square unit cell and in c), Si atom is at the center of the square unit cell

tional tetragonal unit cell with 2 $MoSi_2$ formula units) in the calculation of the γ_s. In Fig. 4, we show total energies for the two (001) surfaces fitted to eq. (9). The asymptotic value of the energy curve in the limit of infinite interplanar separation, taking as the zero of the energy scale the minimum energy (bulk energy), gives the surface energy γ_s. Our results show that binding between (001) Si planes ($\gamma_s = 2.74$ J/m^2) is weaker than that between (001) Mo and Si planes ($\gamma_s = 3.94$ J/m^2). Since the surface relevant to brittle failure is that with the smaller γ_s, we shall focus on the energetics of cleavage between (001) silicon planes in the alloy calculations below.

To obtain a microscopic picture of bonding and better understanding of the above results, we examine the electronic charge densities on various planes of $MoSi_2$. In Fig. 5a, we show contour plots of the electronic charge density on a (110) plane, which contains all the bonds that are broken for cleavage on the (001) plane. Due to the contribution from core 4s and 4p electrons, there is large electronic density at Mo sites, indicated by circular contours which are very closely spaced. Clearly, there is directional bonding between nearest neighbor Mo and Si atoms which is evident from the triangular (anisotropic) regions, indicating local concentration of electrons that form the covalent part of the bond. In contrast, there is no significant covalent bonding between Si–Si and Mo–Mo atoms. This naturally results in lower cleavage energies for (001) planes that separate Si planes. We also display charge densities on (001) planes in Figs. 5b and c. For both Mo and Si (001) layers, the charge densities are nearly isotropic, which, in addition to the small variation in charge density on Si layers, indicates the metallic character of bonding.

Slip systems: The atomic arrangement on the (013) plane is shown in Fig. 6a with the two smallest Burgers vectors, $\mathbf{b}_0 = \frac{1}{2}[131]$ and $\mathbf{b} = \frac{1}{2}[331]$. This plane is treated as a basal plane of a supercell used in the calculation of the stacking fault energy surface. We considered supercells with two and three (013) atomic planes to check convergence of the results with respect to supercell size, for a few points on the γ-surface. All the results for the γ-surface presented here have been obtained with a 3-layer supercell,

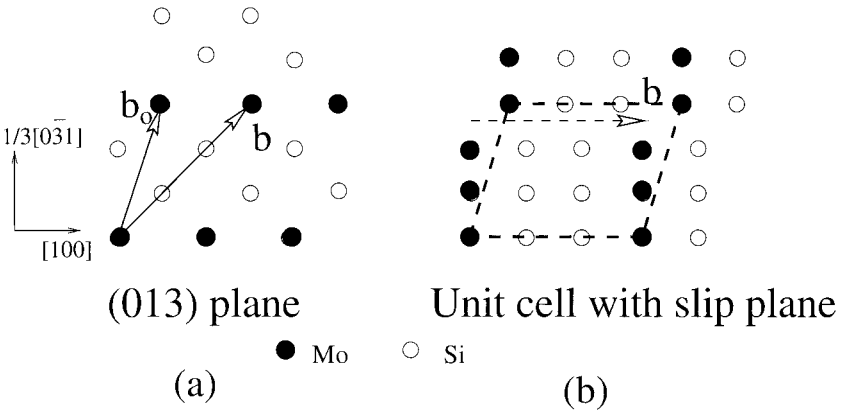

Fig. 6. a) Atomic arrangement in the (013) plane and the two smallest Burgers vectors. b) Schematic geometry of the 3-layer supercell (side view) used in the calculation of slip energies. The dashed arrow indicates displacement of the upper half relative to the lower half of the crystal along a Burgers vector. The thick dashed line indicates the boundary of the supercell corresponding to a finite relative slip of the two halves

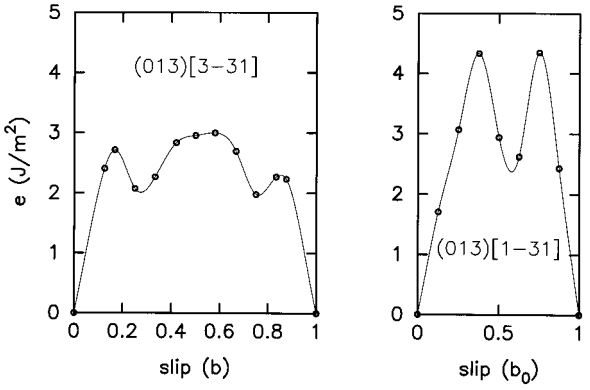

Fig. 7. Energy per unit area of slips on the (013) plane of $MoSi_2$ in (131) and (331) directions, corresponding to the two vectors shown in Fig. 6a. The lines through the points are cubic spline fits

shown in Fig. 6b. In Fig. 7 we show cross-sectional branches of the generalized stacking fault energy surface along the two Burgers vectors. We find $\gamma_{us} = 4.33$ J/m^2 for the slip system $\{013\}\langle 131\rangle$ and $\gamma_{us} = 2.99$ J/m^2 for the slip system $\{013\}\langle 331\rangle$, showing that the nucleation of dislocations on the latter system is energetically favored, despite the longer Burgers vector. The intermediate energy minima along these curves indicate possible stable stacking faults. The connection between these results and possible dislocation dissociation and anti-phase boundary faults in $MoSi_2$ is the subject of Ref. [38].

Substitutional alloys: So far we determined the properties of the cleavage and slip systems relevant to the ductile–brittle transition in $MoSi_2$ using a combination of first-principles calculations and experimental information for the relevant planes. In order to study the effects of substitutional alloying on ductility, we calculate the surface and unstable stacking fault energies for these planes using ordered supercells with a few of the Si or Mo atoms substituted by other elements. The goal here is to examine the effects of a specific alloying element on the bonding in $MoSi_2$ through changes it induces to the disembrittlement parameter D, while ignoring the effects of disorder in such alloys by necessity since quantum mechanical calculations can be performed only for ordered structures with relatively small unit cells.

First we study the effects of Al substitution for Si in detail. We replace a single (001) plane of silicon atoms with aluminium and calculate the surface energy of various (001)

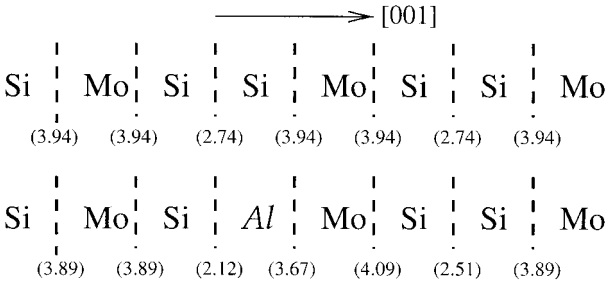

Fig. 8. Schematic representation of the $MoSi_2$ crystal. Each element symbol represents an entire (001) plane of atoms of this type, while the dashed lines represent cleavage planes. The numbers in parentheses are the calculated surface energies (γ_s) for cleavage on those planes. The representation and numbers at the bottom are for a crystal with an entire Si plane near the middle of the slab substituted by Al

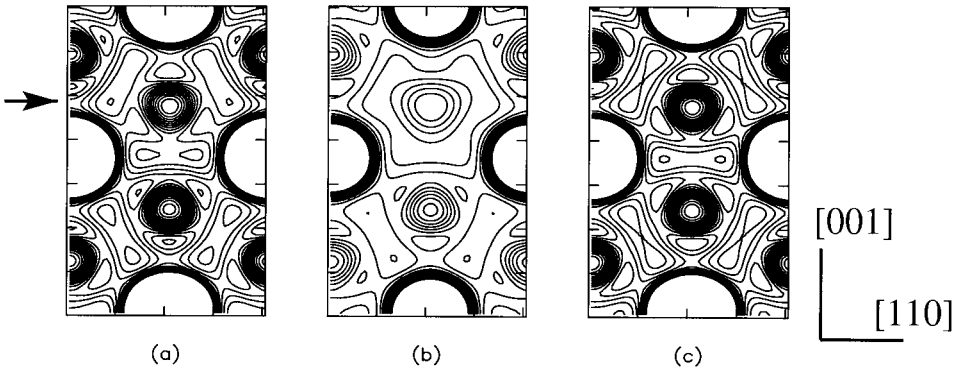

Fig. 9. Electronic charge densities on the (110) plane of Al-substituted $MoSi_2$ with a) 50% and b) 100% planar substitution (Al atoms are substituted in the third atomic layer from the top indicated by an arrow). For comparison, we display the charge density of monolithic $MoSi_2$ in c)

planes, shown schematically in Fig. 8. We find that γ_s for most of the (001) cleavage planes is reduced by Al substitution. The effects on the γ_s for cleavage at Si–Si planes are much stronger than those for cleavage at Mo–Si planes. These effects are strongly localized, decaying rapidly with the distance away from the plane of Al substitution. To obtain a microscopic picture, we examine the electronic charge densities for Al substitution (at 50% and 100% of a plane) which are shown in Fig. 9. This amount of Al substitution corresponds to 16% and 33% substitution by volume or 4.4% and 8.9% substitution by weight, respectively. Comparison to the ideal $MoSi_2$ crystal, included in Fig. 9c, reveals that the changes in charge densities are localized near the plane of Al substitution. These effects become stronger with concentration of planar substitution. The covalent bonding of Si atoms in the plane of substitution with neighboring atoms gets substantially reduced, hence the value of γ_s for cleavage near these planes is more severely affected than for other planes.

The unstable stacking fault energies for Al-substituted $MoSi_2$ are obtained by replacing half or all of the Si atoms in the operative (013) slip plane. With 100% planar substitution (33% by volume) of aluminum for silicon, γ_{us} is reduced by 29%. These calculations did not include atomic relaxation. To estimate the effects of relaxation, we calculated the energy of a configuration corresponding to the highest energy barrier,

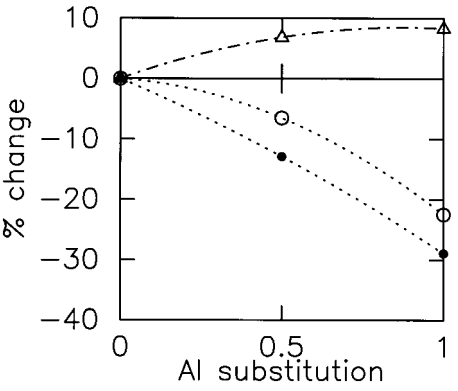

Fig. 10. Percentage change in γ_s (open circles), γ_{us} (closed circles), and D (open triangles) as a function of planar concentration of Al substitution. The lines connecting these points are guides to the eye

Table 2
Effects on γ_s and γ_{us} of full planar substitution of Si by Mg, Al, Ge, and P. D is the disembrittlement parameter and D_0 its value for the ideal crystal ($D_0 = 0.92$)

element	γ_s (J/m^2)	γ_{us} (J/m^2)	$(D - D_0)/D_0$
Si	2.74	2.99	0.00
Mg	1.61	1.45	0.21
Al	2.12	2.13	0.08
Ge	2.32	3.05	−0.17
P	1.78	2.58	−0.26

and find that while the atomic relaxation reduces γ_{us} by 12 to 20%, the percentage reduction in γ_{us} (relative to its value in the ideal crystal) due to Al-substitution remains essentially unchanged. We have also studied how the effects of Al-substitution on γ_s and γ_{us} change with the concentration. We calculated these quantities for 0% (pure $MoSi_2$), 50%, and 100% planar concentrations of Al; the results are shown in Fig. 10. The reduction in γ_{us} (shown as filled circles) varies nearly linearly with Al concentration. The percentage reduction in γ_{us} is larger than that in γ_s for all the concentrations considered and particularly for small concentrations; consequently, the disembrittlement parameter D is enhanced as shown in Fig. 10.

We conducted a more limited investigation into the effects of substitution of Mg, Ge and P for silicon. The results for γ_s and γ_{us} with full planar substitution are summarized in Table 2. It was found that both γ_s and γ_{us} decrease for substitution by Mg and P. For Ge, γ_s decreases but γ_{us} increases slightly. Overall, the disembrittlement parameter D decreases with the number of valence electrons in the substituted element, indicating that alloying with acceptor elements should be better for the enhancement of ductility than alloying with isoelectronic or donor elements. Additional results (Fig. 11) for γ_{us} for substitution with these elements at 50% substitution reveal that, in general, γ_{us} varies to a good approximation linearly with concentration.

Finally we explored the effects of substituting V, Nb, Tc, and Re for Mo. The results for γ_s and γ_{us} are presented in Table 3. As we have shown above, brittle failure breaks Si–Si bonds; therefore substitution for Mo has little effect on γ_s. On the other hand, strong Mo–Si bonds are broken during dislocation nucleation, and hence any substitu-

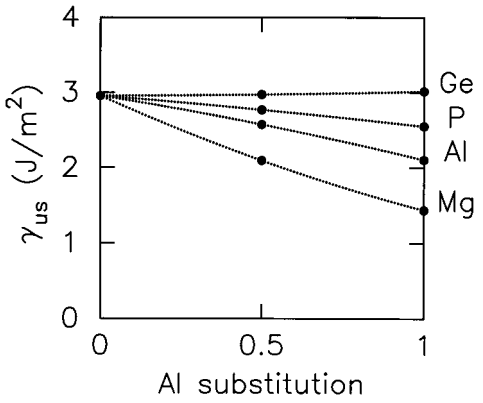

Fig. 11. γ_{us} as a function of planar concentration of Mg, Al, Ge, and P substitution for Si. The lines connecting these points are guides to the eye

Table 3
Effects on γ_s and γ_{us} of full planar substitution for Mo with V, Nb, Tc, and Re

element	γ_s (J/m^2)	γ_{us} (J/m^2)	$(D - D_0)/D_0$
Mo	2.74	2.99	0.00
V	2.49	2.30	0.18
Nb	2.60	2.42	0.18
Tc	2.35	2.34	0.10
Re	2.25	2.55	−0.04

tion for Mo which weakens these bonds should and does lead to a reduction in γ_{us} comparable to that found in the substitution for Si. The disembrittlement parameter D increases with V, Nb, and Tc substitutions, although, as for Si substitution, the effect is weaker for the alloying elements with a higher valence charge. D decreases slightly with substitution of Re for Mo. The effects of V and Nb substitution on D are very similar, because of their same valence.

In Fig. 12, we display charge densities on (110) planes for the cases of 50% substitution of Mo by V and Tc, and compare them to the ideal $MoSi_2$ crystal charge density. In contrast with the substitutions for Si, the effects on charge density seem more extended here. The covalent nature of Mo–Si bonds persists, but is somewhat weakened. This is consistent with the small changes in γ_s we find with these substitutions. The effect of V substitution for Mo on the bonds with nearest neighbor Si atoms is found to be stronger than that of Tc substitution for Mo.

5. Discussion and Conclusions

The interpretation of macroscopic mechanical properties such as ductility and brittleness in terms of fundamental cohesive properties is a complex and difficult task. The present work uses a highly simplified treatment, which borrows heavily from fracture mechanics and dislocation theory, to make the connection between the macroscopic properties and the microscopic structure and composition; first-principles quantum mechanical calculations are used to obtain reliable values for the crucial quantities that enter in the fracture mechanics analysis.

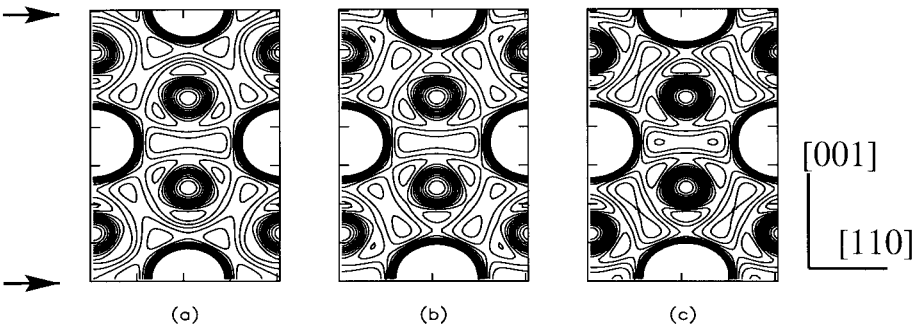

Fig. 12. Electronic charge densities in the (110) plane of a) V-substituted and b) Tc-substituted $MoSi_2$ (V and Tc atoms are substituted for Mo atoms in the top and the bottom layers indicated by arrows). For comparison, we display the charge density of monolithic $MoSi_2$ in c)

There are many approximations and simplifications inherent in this approach. For example, in our analysis of the effects of micro-alloying on the ductility of $MoSi_2$, we assume that the crystal structure of the alloys is the same as that of the matrix material; we have also assumed that the alloying element is readily soluble in the host material. In a similar vein, the sheer numerical complexity of the quantum mechanical calculations, even for this simple model, has forced us to use small supercells which correspond to large concentrations and ordered lattice sites for the alloying elements, even though our stated intention was to look at the *microalloy* regime. We make no attempt to justify these approximations, but rationalize them with the above-mentioned philosophy of providing the most useful and relevant information within the constraints of a real problem. Our results show trends for ductility which can be correlated with electronic structure, and which we expect to provide a cost-effective guide to experiment. We would especially like to emphasize that we were not aware of the recent experimental work [39, 40] confirming our calculated trends with aluminum substitution until after the present calculations were completed. This experimental confirmation is particularly gratifying in light of the drastic approximations employed. We wish to suggest that tests of substitutional microalloys which are predicted to enhance brittleness of $MoSi_2$ (such as Ge or P substituting for Si or Re substituting for Mo) would be particularly useful in providing additional confirmation for the theoretical approach employed here.

In conclusion, through the use of a simple model for ductile versus brittle response, first-principles calculations can be a valuable tool for obtaining microscopic insights into the mechanical behavior of solids. We illustrated this point with an example application to a prototypical brittle solid, silicon. In addition, we illustrated how this approach can be used to provide a guide for experimental efforts to disembrittle a material, molybdenum disilicide, which is of interest for real applications. With ongoing advances in computational resources and algorithms for materials modeling, we expect that the applicability of first-principles methods to modeling and design of materials will become broader.

Acknowledgements This work was performed with support from the Office of Naval Research under SBIR contract no. N00014-97-C-0104. The authors wish to acknowledge significant collaborations with V. V. Bulatov and J. R. Rice, and useful discussions with J. J. Petrovic (Los Alamos National Laboratory) and R. J. Hecht (Pratt & Whitney).

References

[1] C. E. Inglis, Trans. Inst. Naval Arch. **55**, 219 (1913).
[2] P. Hohenberg and W. Kohn, Phys. Rev. **136**, B864 (1964).
W. Kohn and L. J. Sham, Phys. Rev. **140**, A1133 (1965).
[3] V. Vitek, Phil. Mag. **18**, 773 (1968).
[4] M. S. Duesbery and V. Vitek, Acta Mater. **46**, 1481 (1998).
[5] J. R. Rice, J. Mech. Phys. Solids **40**, 239 (1992).
[6] R. Peierls, Proc. Phys. Soc. London **52**, 34 (1940).
[7] F. R. N. Nabarro, Proc. Phys. Soc. London **59**, 256 (1947).
[8] J. P. Hirth and J. Lothe, Theory of Dislocations, Wiley, New York 1982.
[9] V. Vitek and M. Yamaguchi, J. Phys. F (Met. Phys.) **3**, 537 (1973).
[10] B. Joos, Q. Ren, and M. S. Duesbery, Phys. Rev. B **50**, 5890 (1994).
[11] V. Bulatov and E. Kaxiras, Phys. Rev. Lett. **78**, 4221 (1997).

[12] B. JOOS and M. S. DUESBERY, Phys. Rev. Lett. **78**, 226 (1997).
[13] A. A. GRIFFITH, Phil. Trans. Roy. Soc. (London) **A221**, 163 (1920).
[14] A. KELLY, W. R. TYSON, and A. H. COTTRELL, Phil. Mag. **15**, 567 (1967).
[15] J. RICE and R. THOMSON, Phil. Mag. **29**, 73 (1974).
[16] J. R. RICE, in: Topics in Fracture and Fatigue, Ed. A. S. ARGON, Springer-Verlag, Berlin 1992; J. Mech. Phys. Solids, **40**, 239 (1992).
J. R. RICE and G. BELTZ, J. Mech. Phys. Solids, **42**, 333 (1994).
[17] P. B. HIRSCH and S.G. ROBERTS, Phil. Mag. A **64**, 55 (1991).
[18] M. KHANTHA, D. P. POPE, and V. VITEK, Phys. Rev. Lett. **73**, 684 (1994).
[19] J. M. KOSTERLITZ and D.J. THOULESS, J. Phys. C (Solid State Phys.) **6**, 1181 (1973).
[20] phys. stat. sol. (b) **217**, No. 1 (2000).
[21] D. M. CEPERLY and B. J. ALDER, Phys. Rev. Lett. **45**, 566 (1980).
J. P. PERDEW and A. ZUNGER, Phys. Rev. B **23**, 5048 (1981).
[22] J. C. PHILLIPS, Phys. Rev. **112**, 685 (1958).
V. HEINE and M. L. COHEN, Solid State Phys. **24** (1970).
[23] A. M. RAPPE, K. M. RABE, E. KAXIRAS, and J. D. JOANNOPOULOS, Phys. Rev. B **41**, 1227 (1990).
[24] H. J. MONKHORST and J. D. PACK, Phys. Rev. B **13**, 5188 (1976).
[25] M. P. TETER, M. C. PAYNE, and D. C. ALLAN, Phys. Rev. B **40,** 12255 (1989).
[26] G. KREESE and J. FURTHMULLER, Comput. Mater. Sci. **6**, 15 (1996).
[27] J. H. ROSE, J. R. SMITH, F. GUINEA, and J. FERRANTE, Phys. Rev. B **29**, 2963 (1984).
[28] E. KAXIRAS and M. S. DUESBERY, Phys. Rev. Lett. **70**, 3752 (1993).
[29] G. H. VINEYARD, J. Phys. Chem. Solids **3**, 121 (1957).
[30] Y. JUAN and E. KAXIRAS, Phil. Mag. A **74**, 1367 (1996).
[31] Y.-M. JUAN, Y. SUN, and E. KAXIRAS, Phil. Mag. Lett. **73**, 233 (1996).
[32] A. K. BHATTACHARYA and J. J. PETROVIC, J. Amer. Ceram. Soc. **74**, 1045 (1992).
[33] J. J. PETROVIC, R. E. HONNELL, T. E. MITCHELL, T. E. WADE, and K. J. MCCLELLAN, Ceram. Eng. Sci. Proc. **12**, 1633 (1991).
[34] T. C. LU, A. G. EVANS, R. J. HECHT, and R. MEHRABIAN, Acta Metall. et Mater. **39**, 1853 (1991).
[35] S. MALOY, A. H. HEUER, J. J. LEWANDOWSKI, and J. J. PETROVIC, J. Amer. Ceram. Soc. **74**, 2704 (1991).
[36] S. RAWAL, Martin Marietta Astronautics, ONR Workshop on MoSi2, Hyannis, June 1995.
[37] K. ITO, H. INUI, Y. SHIRAI, and M. YAMAGUCHI, Phil. Mag. A **72**, 1075 (1995).
[38] U. V. WAGHMARE, V. BULATOV, E. KAXIRAS, and M. S. DUESBERY, Phil. Mag. A **79**, 655 (1999).
[39] P. PERALTA, S. A. MALOY, F. CHU, J. J. PETROVIC, and T. E. MITCHELL, Scripta Mater. **37**, 1599 (1997).
[40] P. PERALTA, F. CHU, S. A. MALOY, P. SANTIAGO, J. J. PETROVIC, and T. E. MITCHELL, Proc. AFOSR-Sponsored Internat. Conf. Computer-Aided Design of High-Temp. Mater., 30 July to 2 August 1997, Santa Fe (New Mexico).